J Sol-Gel Sci Technol (2014) 70:422–427
DOI 10.1007/s10971-014-3302-z

ORIGINAL PAPER

Effects of Pb^{2+} ions concentration on the structure and PL intensity of Pb-doped $ZnAl_2O_4$ nanocrystals synthesized using sol–gel process

S. V. Motloung · F. B. Dejene · H. C. Swart · O. M. Ntwaeaborwa

Received: 29 August 2013 / Accepted: 7 February 2014 / Published online: 15 February 2014

Abstract Undoped and Pb^{2+}-doped ultrafine cubic zinc aluminate ($ZnAl_2O_4$) hosts were successfully prepared at a relatively low temperature (~80 °C) using the sol–gel method. The concentration of Pb^{2+} was varied from 0 to 5 mol%. The TGA showed that the minimum annealing temperature required to obtain single phase $ZnAl_2O_4$ must be above 400 °C. The XRD data revealed that all the annealed samples were single phase crystalline structures and the estimated crystallites size were in the range of 21–30 nm in diameter. The FTIR results suggest that heat-treating can destroy some of the bonds. The surface morphology of the phosphors was influenced by the Pb^{2+} mol%. Undoped and Pb^{2+}-doped $ZnAl_2O_4$ nanoparticles exhibit the violet emission at slightly different positions. The slight peak shifts suggests the possibilities that the luminescence centre can either be due to the defects level in the host or Pb^{2+} ions. The emission peaks at 390 and 399 nm are ascribed to the typical UV transitions $^3P_{0,1} \rightarrow {}^1S_0$ in Pb^{2+} ion. At the higher Pb^{2+} mol%, the luminescence quenching behaviour occurs, which suggests that doping with Pb^{2+} ions is accompanied by the introduction of new defect sites that enhance non-radiative recombination of the excited electrons.

Keywords Sol–gel · $ZnAl_2O_4$ · Pb^{2+} mol% · Pb^{2+} luminescence

S. V. Motloung (✉) · F. B. Dejene
Department of Physics, University of the Free State (Qwaqwa Campus), Private Bag X13, Phuthaditjhaba 9866, South Africa
e-mail: motloungsv@qwa.ufs.ac.za

H. C. Swart · O. M. Ntwaeaborwa
Department of Physics, University of the Free State, P.O. Box 339, Bloemfontein 9300, South Africa

1 Introduction

Doped and undoped semiconductor nanoparticles have received major interest in the scientific community because of their unique and superior properties, such as size-dependent optical properties [1]. $ZnAl_2O_4$ is one of the wide-band gap (~3.8 eV) semiconductors being considered for the photoelectronic devices, UV-transparent conductor, sensor, and dielectric material [2–4]. $ZnAl_2O_4$ have the chemical formula AB_2O_4, where A is Zn^{2+} ion that occupies a tetrahedral and B represent Al^{3+} ion which occupies octahedral sites of a cubic crystal [5]. $ZnAl_2O_4$ and other spinels are known to be suitable host lattice for various dopants or activator atoms [6, 7]. For instance, there have been several reports on the rare earth and transition metal ions doped $ZnAl_2O_4$ phosphor, and most of these studies focus more on the well known luminescing dopants such as Mn^{2+}, Eu^{2+}, Tb^{3+}, etc. [3]. Apart from the rare earths and transition metal, a group of so called heavy ns^2 metal ions such as Tl^+, Pb^{2+} and Bi^{3+} luminescing dopants have been studied in a considerable number of hosts [8, 9]. In particular, the luminescence of the Pb^{2+} ion is quite diverse and strongly depends on the environmental condition of Pb^{2+} in a host lattice [10, 11]. The nature of Pb^{2+} ion luminescence in complex oxides usually consists of emission bands in the UV and visible ranges [12]. The UV emission is ascribed to the $^3P_{0,1,2} \rightarrow {}^1S_0$ transition in the Pb^{2+} monomer center. While the visible emission is ascribed to emission from the D-level, which is believed to originate from a charge transfer transition [10, 13].Many fabrication methods of $ZnAl_2O_4$ phosphor such as solid state reaction [14], co-precipitation [15], hydrothermal [16], combustion [17] and sol–gel [18] have been developed. As an alternative, in this work, we have adopted the sol–gel method [18], which is known to be a

low-temperature technique, in order to obtain a low cost green phosphor for use in applications such as X-ray imaging device, low pressure lamps, and high-energy physics [18]. In view of these, this paper, reports on the sol–gel synthesis of undoped and Pb^{2+}-doped $ZnAl_2O_4$ at a very low temperature (~80 °C). The effects of Pb^{2+} content at a range of 0–5 mol% on the structural and luminescence properties were investigated with the aim of fabricating UV down-conversion phosphor materials that can be used in different types of light emitting devices.

2 Experimental

The undoped and Pb^{2+}-doped $ZnAl_2O_4$ nanocrystals were synthesized using a well-known sol–gel technique [18]. $Zn(NO_3)_2{\cdot}6H_2O$ (98 %), $Al(NO_3)_3{\cdot}9H_2O$ (98.5 %) and Citric acid, $C_8H_8O_7{\cdot}H_2O$ (99 %) were dissolved in deionized water. The sols stoichiometric molar ratio of Zn:Al was 2:1. Specified amounts of $Pb(NO_3)_2$ was added in the solution to dope with different mol% of Pb^{2+} ions. The Pb^{2+} content was varied at the range of 0–5 mol%. In all samples, the heating temperature was kept below 80 °C while constantly stirring on a magnetic stirrer until the transparent gels of the mixed metal citrates were formed. The gels were dried at room temperature for 2 days and then in an oven kept at a temperature of 145 °C. The white dried gels were ground into fine powders and were subsequently annealed at 800 °C in a furnace for an hour. The samples were then taken for the characterization. Thermogravimetric analysis was carried out using a Perkin Elmer TGA7 in the temperature range of 20–580 °C at a heating rate of 10 °C/min under an air flux. The stretching mode frequencies were determined using a Perkin Elmer Spectrum 100 FTIR spectrometer. The crystal structure of the samples was characterized by X-ray powder diffraction (Bruker AXS Discover diffractometer) with CuKα (1.5418 Å) radiation). The surface morphology of the phosphor powders was analyzed using a Shimadzu Superscan ZU SSX-550 scanning electron microscope (SEM). Photoluminescent spectra were recorded at room temperature using a Hitachi F-7000 fluorescence spectrophotometer.

3 Results and discussion

3.1 Thermogravimetric analysis

Figure 1 shows the thermal decomposition of the as prepared $ZnAl_2O_4$ (host) gel. Several thermal features take place during the heating of the gel. As anticipated the variation of the mass of the compound with temperature indicates slow weight loss up to 80 °C due to the release of

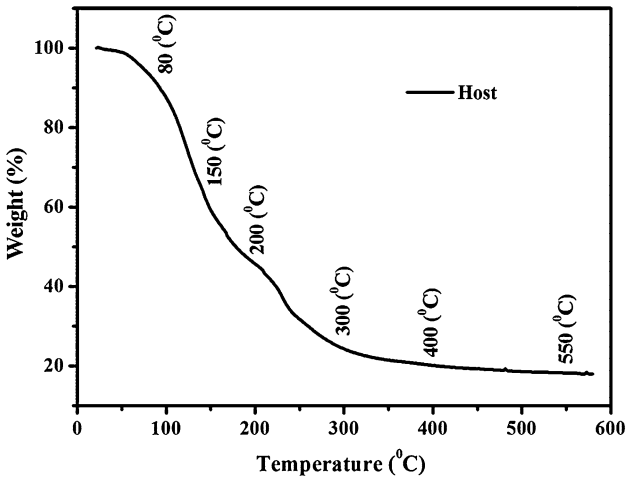

Fig. 1 TGA curve of $ZnAl_2O_4$ gel obtained with the heating rate of 10 °C/min

interlayer water [4, 19]. An event at around 150–200 °C, is attributed to the expulsion of hydrated water [4, 19, 20]. The last event at around 300–400 °C is attributed to the elimination of organic compounds and starting of crystallization process and the formation of single phase $ZnAl_2O_4$ [4, 19].

These results suggest that the minimum annealing temperature to start obtaining cubic phase $ZnAl_2O_4$signature is 400 °C with high chances of forming other oxides impurities such as ZnO and Al_2O_3. Thus, the annealing temperature must be higher than 400 °C to completely eradicate impurities and enhances the crystallinity of the single phase $ZnAl_2O_4$. TGA results are consistent with what is observed in the XRD and FTIR analysis.

3.2 X-ray diffraction

The crystallinity of the powder samples prepared by sol–gel method was determined by means of XRD. To reveal the structural properties of the un-doped and Pb^{2+}doped $ZnAl_2O_4$, the XRD patterns are presented in Fig. 2. The XRD pattern is consistent with the standard data for the cubic $ZnAl_2O_4$ spinel phase (JCDPS: 82-1043). The results clearly reveal that highly crystalline cubic $ZnAl_2O_4$ single phase can be obtained after annealing at 800 °C. This is supported by the fact that there were no extra peaks of impurities related to ZnO or Al_2O_3. The same phases without impurities were observed for all Pb^{2+}doped samples at the range of 0–5 mol%. Thus, it is highly believed that the Pb^{2+} ions were fully incorporated into the host matrix. The results suggest that varying the mol% of Pb^{2+} ions does not affect the crystal structure of the phosphor. The crystallites sizes were estimated by using the Scherrer formula [21], using the most intense peak, and were found to be 22, 29, 21, 30 and 22 nm for the 0, 0.25, 1, 3 and 5 %

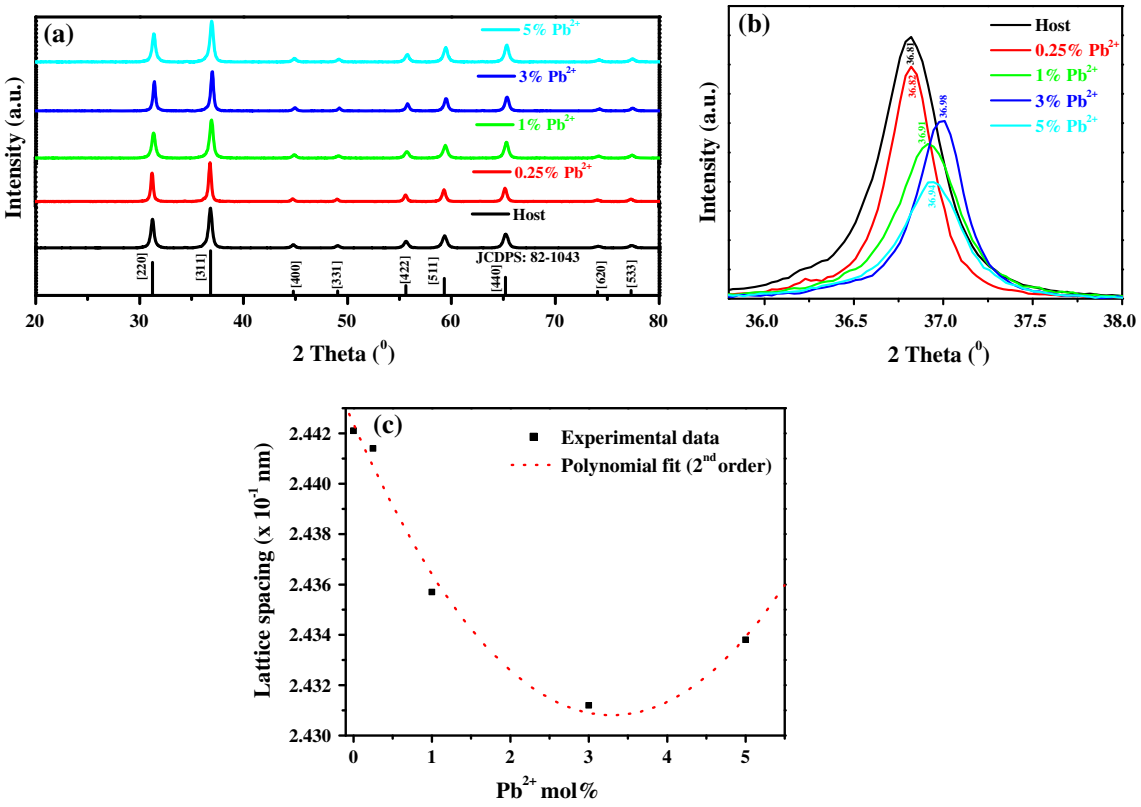

Fig. 2 X-ray patterns of the **a** un-doped and Pb^{2+} doped $ZnAl_2O_4$ phosphors and **b** analysis of (311) diffraction peak and **c** lattice spacing as a function of Pb^{2+} mol%

Pb^{2+} ions, respectively. Furthermore, when considering the most intense diffraction peak (311) shown in Fig. 2b, it can be seen that there is a peak shift to the higher angle and decrease in diffraction intensity with an increase in Pb^{2+} mol% concentration. This relationship in our results is consistent with what has been reported by Hou et al. [22] in the study of electrical and optical properties of Al doped ZnO and $ZnAl_2O_4$. The average lattice spacing was estimated to be 0.24 nm, which corresponds with (311) lattice spacing of the $ZnAl_2O_4$ reported by Zawadzki et al. [23]. As expected, shifting to the higher angle is attributed to the decrease in the lattice spacing as the Pb^{2+} ions are incorporated into the $ZnAl_2O_4$ matrix (see Fig. 2c). This is due to the substitution of Zn^{2+} (ionic radius 0.74 Å) [22] with bigger Pb^{2+} (ionic radius 1.01–1.40 Å) [24] ions. In general, it is assumed that when a cation is replaced by other larger, the result is an expansion of the lattice and therefore both the interplanar d-spacing increases and the 2θ is shifted to lower angle. So, the mechanism of Pb^{2+}-doped $ZnAl_2O_4$ solid solution formation must be different. May be it could include anionic vacancy formation.

Lubarda et al. [25] observed similar results deviating from Vergard's law when replacing Au atoms (1.5939 Å) with Ag atoms (1.5969 Å) in the Ag–Au alloy. The variation of the lattice spacing of the (311) diffraction peak, shows (in Fig. 2c) the parabolic behaviour relationship to the Pb^{2+} mol%. The decrease in lattice spacing in our study is, therefore, attributed to the shrinkage of the Pb^{2+} outer electron shell due to its electronic interactions with more neighbouring Zn^{2+} ions, which makes it smaller than the Zn^{2+} ion [25]. As the Pb^{2+} mol% is increased further, the shrinkage is expected to be less pronounced (due to the additional Pb^{2+} ions), as a results, the lattice spacing is expected to recover or increase and this serves as a motivation why there is an increase in lattice spacing at 5 % Pb^{2+}. These can also be a relevant reason why Lubarda et al. [25] observed high increase in lattice spacing at higher mol% of the Ag. Lubarda et al. [25] results and our results suggest that for some materials, at a low mol% of the dopant, the Vergard's law is not favoured. Thus, it is concluded that there is an optimum mol% required for the Vergard's law to occur. The second order polynomial fit in Fig. 2c shows that the 3.4 % Pb^{2+} is an optimum for our results to behave as expected by Vergard's law. The decrease of the (311) diffraction peak intensity as the Pb^{2+} mol% is increased can be explained to be due to the replacement of smaller with bigger atoms, which destroys the crystal quality. The destruction of crystal quality is expected to be more pronounced as bigger foreign atoms are incorporated and this is supported by our findings in

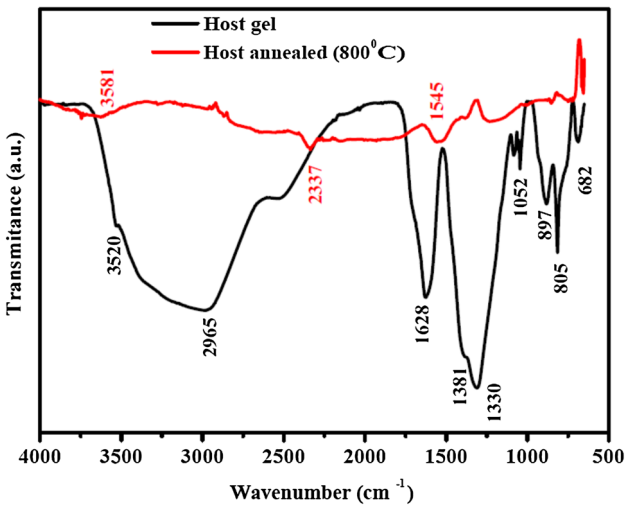

Fig. 3 FTIR spectra of the undoped $ZnAl_2O_4$ (host)

Fig. 2b. It is therefore concluded that the Pb^{2+} mol% influences the particle size growth, the lattice spacing and crystal quality.

3.3 FTIR

Figure 3 shows the FTIR spectra of the un-doped $ZnAl_2O_4$ gel and annealed at 800 °C powder. The band at 682 cm^{-1} is assign to the stretching vibration of tetrahedral and octahedral bonds in the spinel [4, 26, 27]. The IR spectra of the gel indicate the presence of nitrates groups at 805, 897 and 1,052 cm^{-1}. The bands at 1,330–1,628 cm^{-1} can be attributed to the OH group in the metal alkoxides present in the gel [27, 28]. The wide absorption band centred at 2,965–3,520 cm^{-1} corresponds to OH group, which is contributed by the water content present in the gel. As far as the annealed sample is concern, the shallow band observed at 3,581 cm^{-1} is assigned to O–H stretching vibration [29]. The band at 2,337 cm^{-1} is attributed to the presence of O–O bonds in the crystal lattice, which is treated as a feature of spinel structured crystallites. Finally, a small band at 1,545 cm^{-1} is attributed to the amide bonds [30]. In comparing the gel and the annealed powder, it can be seen that the number of bands decreases when the samples were annealed at 800 °C, suggesting that the annealing temperature destroys most of the bonds, which suggests the formation of the single phase $ZnAl_2O_4$ as shown by the XRD results.

3.4 SEM

The surface morphologies of the samples annealed at 800 °C for the undoped, 1 and 5 % Pb^{2+}-doped $ZnAl_2O_4$ are shown on SEM micrographs in Fig. 4a–c, respectively. The undoped powder composed of small spherical and chunk granular particles dispersed all over the surface. The 1 % Pb^{2+}-doped sample shows rough particle agglomerates with voids distributed in the matrix. It is, therefore, proposed that the rough particle agglomerates with voids might lead to easy escape routes to the emitted light with the consequent increase in the light output. The 5 % Pb^{2+}doped sample shows the particle-to-particle separation and more grain boundaries-like-porous structures distribution on the surface.

3.5 Photoluminescence analysis

Figure 5a shows the PL excitation and emission spectra. It was observed that the main peaks of excitation when monitoring the UV emission at 395 nm are at 285 and 332 nm. Both absorption bands are attributed to the host absorption [26]. The emission spectra reveal that both undoped and Pb^{2+}-doped $ZnAl_2O_4$ powders exhibit UV emission peaks at slightly different positions 390, 395 and 399 nm. Note that within the investigated range of 0–5 mol%, the 1 % Pb^{2+} had the highest emission intensity. The emission intensity as a function of Pb^{2+} mol% is presented in Fig. 5b. The Gaussian fit suggests that the optimum dopant concentration of these nanoparticles must be at 1.5 % Pb^{2+}. Above this optimum concentration, the concentration quenching effect on the emission intensity is observed. Similar quenching in luminescence intensity has been observed in TiO_2 doped with In- and Ce- by Tang et al. [31] and for TiO_2 doped with Pb- by Rahman et al. [32]. Thus, it is strongly believed that doping at higher Pb^{2+} mol% introduces new defect sites that enhance non-radiative recombination of the excited electrons. Furthermore, the small shift in peak position indicates that the UV emission can be from either the host or Pb^{2+} ions. The emission from the host at 395 nm is ascribed to be due to the intrinsic intrabandgap defects, such as oxygen vacancies (V_0^*) [4, 26] as shown inFig. 6b. Da Silva et al. [4] suggested that these defects provide donor levels near the conduction band edge of the oxide.

The luminescence mechanism taking place for all emission arising from the undoped and Pb^{2+}-doped $ZnAl_2O_4$ are illustrated in Fig. 6. The electrons in the ground state are excited to the conduction band after the excitation of 285 nm. As far as the host emission is concerned, the excited electrons are de-excited by non-radiative relaxation (NRR) and trapped on the defect states (V_0^*), and then de-excited to the valence band by radiative decay. The incorporation of Pb^{2+} into the $ZnAl_2O_4$ matrix can be interpreted as a development of more new trapping centers [1]. For the emission from the Pb^{2+}, it is proposed here that the mechanism is exactly similar to that one of the host emission but the difference is the trapping centers. As shown in Fig. 5a, the emission from the Pb^{2+} doped

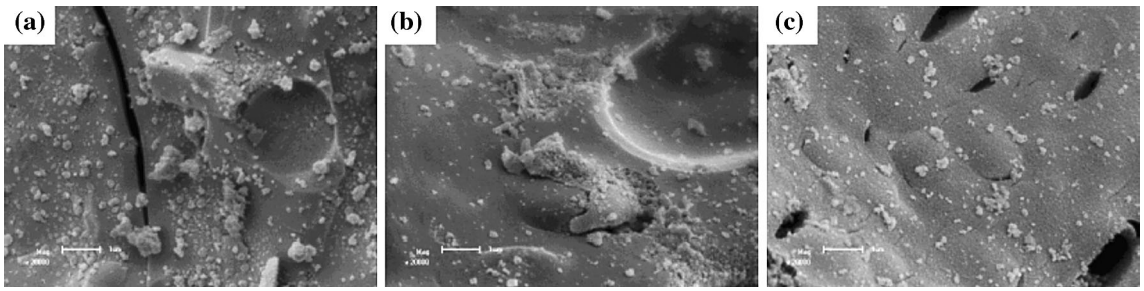

Fig. 4 SEM micrographs for the **a** $ZnAl_2O_4$ (host), **b** 1 % Pb and **c** 5 % Pb^{2+}

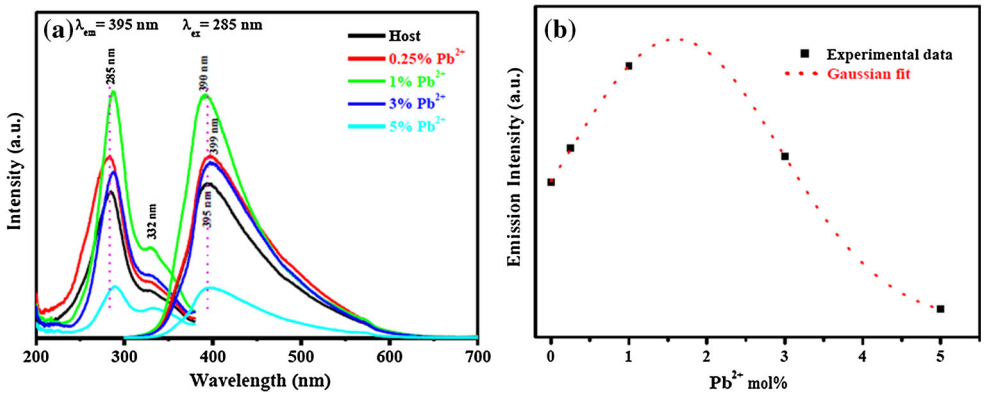

Fig. 5 **a** Excitation and emission spectra of the undoped and Pb^{2+}-doped $ZnAl_2O_4$ at different Pb^{2+} mol%. **b** Variation of emission intensity as a function of Pb^{2+} mol%

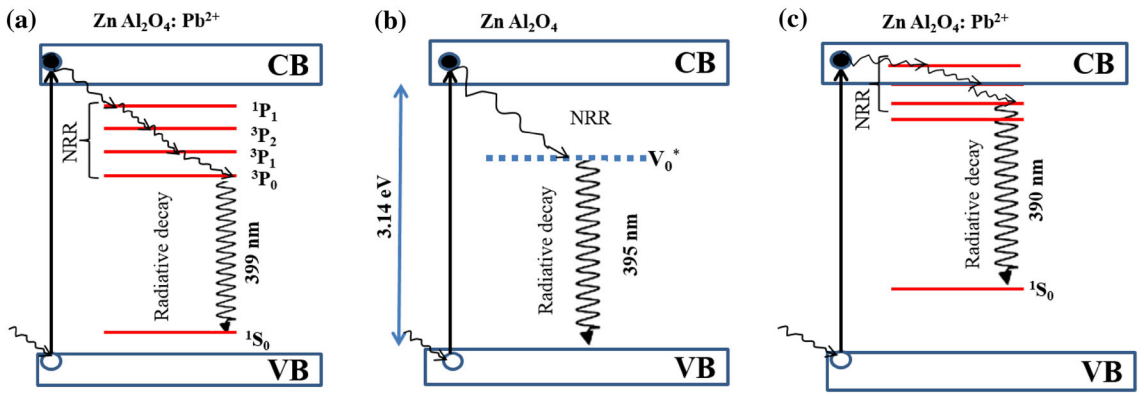

Fig. 6 Energy levels diagram mechanism for the **a** $ZnAl_2O_4$: Pb^{2+} emission at 399 nm, **b** undoped $ZnAl_2O_4$ emission at 395 nm and **c** $ZnAl_2O_4$: Pb^{2+} emission at 390 nm

$ZnAl_2O_4$ are slightly at different positions, which are at 390 and 399 nm. These shifts of the emissions peaks towards the shorter and higher wavelength suggest that the emission must be from different transitions in Pb^{2+} ion. Mehnaoui et al. [33] made an attempt to identify the pure electronic transitions between the ground and the excited levels of Pb^{2+} ion. In their study [33], they were successful to show that Pb^{2+} ions can occupy two different sites in the apatite and that leads to the probabilities of having two distinct emissions from the lower $^3P_1 \rightarrow {}^1S_0$ and higher $^3P_0 \rightarrow {}^1S_0$ energy transitions, which are associated to the Pb^{2+} ion. It is therefore, reasonable to draw-up the conclusion that these two emission bands from this report must originate from slightly different energy levels transitions from Pb^{2+} ion as shown in Fig. 6a, c. The emission at the higher wavelength (lower energy), 399 nm, is assign to be from the $^3P_0 \rightarrow {}^1S_0$ transition [12, 33], which must be within the host bandgap with possibilities of NRR and radiative decay. Finally, the emission from the lower wavelength, 390 nm, (higher energy) is attributed to the $^3P_1 \rightarrow {}^1S_0$ transition induced by Pb^{2+} ion. In this case, because of the bandgap energy ($\sim$3.18 eV), it is proposed that some of the Pb^{2+} energy levels are trapped within the conduction band of the host (since the host band gap is 3.14 eV see Fig. 6b). Thus, it is concluded that the Pb^{2+} doping results in the modification of the bandgap energy

and defects levels within the host matrix. As anticipated, the emission from the Pb^{2+} energy level trapped within the conduction band has the maximum intensity as shown in Fig. 5a. Note that the lifetime and afterglow spectrum were not gathered and therefore they are not discussed in this report.

4 Conclusions

The X-ray diffraction data revealed that the annealed samples consist of highly crystalline cubic $ZnAl_2O_4$. Varying the mol% of Pb^{2+} ions does not affect the crystal structure of the phosphor. The shifting of the 311 reflection into the higher angle is attributed to the decrease in the lattice spacing. The results also suggest that the good particle agglomeration and voids leads to an easy escape routes to the emitted light with the consequent of enhancing the luminescence of a phosphor. The PL results demonstrated that undoped and Pb^{2+} impurities activated $ZnAl_2O_4$ emits at slightly different UV positions. It is concluded that the emission can be from either the host or Pb^{2+} ions. The incorporation of Pb^{2+} ions influences the defects levels position and bandgap energy. At the higher Pb^{2+} mol%, the luminescence quenching behaviour occurs due to the introduction of more new defect sites that enhance non-radiative recombination of the excited electrons.

Acknowledgments This work is supported by the South African National Research Foundation (NRF) and the research fund of the University of the Free State. The PL system used in this study is supported both technically and financially by the rental pool programme of the National Laser Centre.

References

1. Borse P, Vogel W, Kulkarni S (2006) J Colloid Interface Sci 293:437
2. Ehlert O, Osvet A, Batentschuk M, Winnacker A, Nann T (2006) J Phys Chem B 110:23175
3. Zhang D, Wang C, Liu Y, Shi Q, Wang W, Zhai Y (2012) J Lumin 132:1529
4. Da Silva AA, Goncalves A, Davolos MR (2009) J Sol–Gel Sci Technol 49:101
5. Ciupina V, Carazeanu I, Prodan G (2004) J Optoelectron Adv Mater 6:1317
6. Singh V, Chakradhar RPS, Rao J, Kim DK (2008) J Lumin 128:394
7. Lakshminarayana G, Wondraczek L (2011) J Solid State Chem 184:1931
8. Nikl M, Novoselov A, Mihokova E, Polak K, Dusek M, McClune B, Yoshikawa A, Fukuda T (2005) J Phys Condens Matter 17:3367
9. Seltur AA, Srivastava AM (2006) Opt Mater 29:410
10. Folkerts HF, Hamstra MA, Blasse G (1995) Chem Phys Lett 246:135
11. Sun Q, Wang J, Shi J (2010) J Solid State Chem 183:1174
12. Zorenko Y, Gorbenko V, Voznyak T, Zorenko T (2008) Phys Statis Solidi B 245:1618
13. Bol AA, Meijerink A (2001) Phys Chem 3:2105
14. Keller JT, Agrawal DK, McKinstry HA (1998) Adv Ceram Mater 3:420
15. Yuan FL, Hu P, Yin CL, Huang SL, Li JL (2003) J Mater Chem 13:634
16. Chen Z, Shi E, Zheng Y, Li W, Wu N, Zhong W (2002) Mater Lett 56:601
17. Adak AK, Pathak A, Pramanik P (1998) J Mater Sci Lett 17:559
18. Wu Y, Du J, Choy K, Hench LL, Guo J (2005) Thin Solid Films 472:150
19. Valenzuela MA, Bosch P, Aguilar-Rios G, Montoya A, Schifter I (1997) J Sol–Gel Sci Technol 18:110
20. Jamal EMA, Kumar DS, Anantharaman (2011) Bull Mater Sci 34:251
21. Cullity BD (1978) 1956 Elements of X-ray diffraction, 2nd edn. New York, Addison Wesley
22. Hou Q, Meng F, Sun J (2013) Nanoscale Res Lett 8:144
23. Zawadzki M (2006) Solid State Sci 8:14
24. Chen SB, Ma YB, Chen L, Xian K (2010) Geochem J 44:233
25. Lumbarda VA (2003) Mech Mater 35:53
26. Da Silva AA, Goncalves A, Davolos MR, Santagneli SH (2008) J Nanosci Nanotechnol 8:5690
27. Jamal EMA, Kumar DS, Anantharaman (2011) Bull Mater Sci 34:251
28. Kuang WX, Fan YN, Yao KW, Chen Y (1998) J Solid State Chem 140:354
29. Bajpai AK, Likhitkar S (2001) Bull Mater Sci 36:15
30. Zhou Y, Bruening ML, Bergbreiter DE, Crooks RM, Wells M (1996) J Am Chem Soc 118:3773
31. Tang H, Berger H, Schmid PE, Levy F, Burri G (1993) Solid State Commun 87:847
32. Rahman MM, Krishna KM, Soga T, Jimbo T, Umeno M (1999) J Phys Chem Solid 60:201
33. Mehnaoui M, Ternane R, Panczer G, Trabelsi-Ayadi M, GBoulon G (2008) J Phys Condens Matter 20:275227